Solid Target production for Astrophysical Reasearch: the European target laboratory partnership in ChETEC-INFRA

RobertaSpartà[1,2], Alexandra Spiridon[3], Rosanna Depalo[4,5], Denise Piatti[6,7], Antonio Massara[2], Nicoleta Florea[3], Marcel Heine[8], Radu-Florin Andrei[3], Beyhan Bastin[9], Ion Burducea[3], Antonio Caciolli[6,7], Matteo Campostrini[10], Sandrine Courtin[8,11], Federico Ferraro[12], Giovanni Luca Guardo[2], Felix Heim[13], Decebal Iancu[3], Marco La Cognata[2], Livio Lamia[14,2,15], Gaetano Lanzalone[1,2], Eliana Masha[16], Paul Mereuta[3], Jean Nippert[8], Rosario Gianluca Pizzone[14,2], Giuseppe Gabriele Rapisarda[14,2], Maria Letizia Sergi[14,2], Jakub Skowronski[6,10], Dana State[3], Tamás Szücs[17], Livius Trache[3], and Aurora Tumino[1,2]

[1] Dipartimento di Ingegneria e Architettura, Università di Enna 'Kore', Enna, Italy
[2] Laboratori Nazionali del Sud, INFN, Catania, Italy
[3] National Institute of Physics and Nuclear Engineering Horia Hulubei, Bucharest-Magurele, Romania
[4] Università degli Studi di Milano, Milano, Italy
[5] Sezione di Milano, INFN, Milano, Italy
[6] Università degli Studi di Padova, Padova, Italy
[7] Sezione di Padova, INFN, Padova, Italy
[8] Université de Strasbourg, CNRS, IPHC UMR 7178, 67000, Strasbourg,, France
[9] Grand Accélérateur National d'Ions Lourds, GANIL, Caen, France
[10] Laboratori Nazionali di Legnaro, INFN, Legnaro, Italy
[11] University of Strasbourg Institute of Advanced Studies, USIAS, Strasbourg, France
[12] Laboratori Nazionali del Gran Sasso, INFN, Assergi, Italy
[13] Institute for Nuclear Physics, University of Cologne, Cologne, Germany
[14] Dipartimento di Fisica e Astronomia "E. Majorana", Università of Catania, Catania, Italy
[15] Centro Siciliano di Fisica Nucleare e Struttura della Materia, CSFNSM, Catania, Italy
[16] Helmholtz-Zentrum Dresden-Rossendorf, Dresden, Germany
[17] Institute for Nuclear Research, ATOMKI, Debrecen, Hungary

Corresponding author:
Roberta Spartà[1]

Email address: rsparta@lns.infn.it

ABSTRACT

The joint work of European target laboratories in the ChETEC-INFRA project is presented, to face the new experimental challenges of nuclear astrophysics. In particular, results are presented on innovative targets of ^{12,13}C, ^{16}O, and ^{19}F that were produced, characterized, and, in some cases, tested under beam irradiation. STAR (Solid Targets for Astrophysics Research) is already acting to increase collaboration among laboratories, to achieve shared protocols for target production, and to offer a characterization service to the entire nuclear astrophysics community.

INTRODUCTION

Reliable and precise nuclear reaction cross section measurements are crucial challenges for nuclear astrophysics. At energies of interest for stellar nucleosynthesis, the cross sections are, indeed, of the order of pb to fb, translating to low experimental yields. Scientist efforts are focused on achieving the required

precision needed for stellar models via both direct and indirect methods.

ChETEC-INFRA (Chemical Elements as Tracers of the Evolution of the Cosmos - Infrastructures for Nuclear Astrophysics - https://www.chetec-infra.eu/) is a European project in the framework of H2020 which networks different types of infrastructure, joining forces and expertise needed to study the origin of the chemical elements.

Nuclear astrophysicists who want to study charged particles induced reactions struggle with the necessity to maximize the signal-to-noise ratio in every possible way, including the target improvement. The development of stable targets for high precision measurements down at astrophysical energies is the main goal of STAR (Solid Targets for Astrophysics Research https://www.chetec-infra.eu/jra/star/) task inside ChETEC-INFRA. Besides the TransNational Access facilities (Felsenkeller laboratory, Bellotti-Ion Beam facility, IFIN-HH (Romania)), the STAR participating institutions are: ATOMKI (Hungary), CNRS (France), IFIN-HH (Romania), INFN (Italy), University of Padua, University of Milan, University Kore (Italy), and University of Cologne (Germany), as shown in Figure 1.
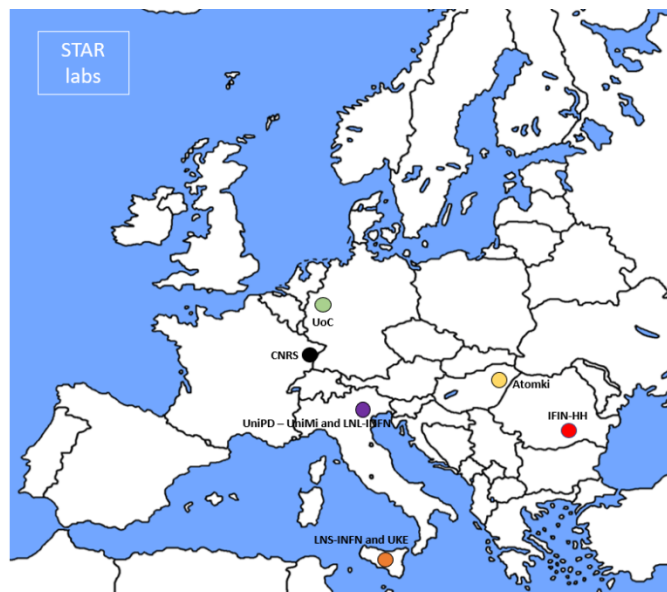
Figure 1. Map of the ChETEC-INFRA STAR task members.

The STAR collaboration aims to develop, test and make protocols of special solid targets complying with the new requirements of experimental studies of reactions of astrophysical interest, namely purity, enrichment, composition, thickness, and stability under irradiation.

To this end, STAR is working towards the realization of:

- ultra-pure material targets for low reaction yields, in which signals from parasitic reactions on impurities can limit experiments and must therefore be reduced.

- noble gases solid targets: being impossible for them to create solid compounds, noble elements are generally used in the form of gas target, but other than their low densities, angular spread and energy loss and straggling can hinder the reaching of the experimental needs in many cases. Thus, He and Ne solid targets, produced by implantation into a host material, would be preferable.

STAR activities are mainly focused on targets suitable for crucial measurements for the astrophysical scenarios of C-burning (sec. 1), s-process (sec. 3) and of physics beyond the Standard Model (sec. 2).

C-burning main process is the $^{12}C+^{12}C$ fusion reaction (sec. 1.1), which plays a key role in the heavy elements nucleosynthesis and for the supernovae (SNe) evolution, significantly affecting the chemical and physical galaxy evolution. At astrophysical energies, $^{12}C+^{12}C$ fusion reaction cross sections are of the order of fb. Present experimental direct data (lowest $E_{c.m.}=2.2$ MeV) are affected by large uncertainties, that are further enhanced when extrapolated to stellar energies, because of the poorly constrained structure of the ^{24}Mg compound nucleus Fruet et al. (2020); Tan et al. (2020); Jiang et al. (2018); Spillane et al. (2007). A recent indirect measurement Tumino et al. (2018) down to low energy has found a resonant behaviour which is also responsible of a huge increase in the reaction rate in the temperature range of interest for superburst (T=0.4-0.5 GK).

To substantiate these results and to put on a firmer ground the normalization of the indirect result, a future measurement is planned by the LUNA collaboration, for which STAR collaborates in the search for the optimal target.

Moreover, also other light ions fusion reactions, as ^{12,13}C+^{16}O or +^{19}F, are under consideration by researchers to investigate the presence of specific reaction mechanisms like the so-called *fusion hindrance* at sub-barrier energies (sec. 1.2 and 1.3).

Highly enriched fluorine targets were produced and tested both for the latter and for the X17 boson Krasznahorkay et al. (2016) search in the NEW JEDI experiment Bastin et al. (2023) through the study of ^{8}Be levels in the 18 MeV energy region, populated via ^{7}Li+p. The proton beam was impinging on a LiF target, hence the need of fluorine targets for the background subtraction. Results are in sec. 2.

The nucleosynthesis via s-process is responsible for the production of about half of heavy elements with A $\leq$ 90. The two main neutron sources are the ^{13}C(α, n)^{16}O and the ^{22}Ne(α,n)^{25}Mg reactions. While the former has been recently measured inside the Gamow Peak Ciani et al. (2021); Gao et al. (2022); La Cognata et al. (2013) the latter is still poorly constrained below the resonance at E$\sim$832 keV (J$^\pi$ = 2$^+$) Jaeger et al. (2001); Harms et al. (1991); Drotleff et al. (1993), where mainly upper limits are reported. Moreover, a crucial parameter to improve our understanding of s-process nucleosynthesis is the ratio between (α,n) and (α,γ) rates, since it determines the temperature at which the neutron production starts to become effective Adsley et al. (2021). STAR studies for solid helium targets for future measurement planned at INFN-LNS are explained in sec. 3.

It is worth to promote that target production and characterization is a service open to the nuclear astrophysics European community (for contacts, see STAR (2021)).

Results achieved in the STAR framework are described in the following sections.

1 C-BURNING AND LIGHT IONS SUB-BARRIER FUSION HINDRANCE OF THE CROSS SECTIONS

The study of fusion reactions occurring at energies below the Coulomb barrier between light ions, especially ^{12}C and ^{16}O (thus ^{12}C+^{12}C, ^{12}C+^{16}O, ^{16}O+^{16}O), holds a large significance in various astrophysical scenarios, spanning from the creation of elements to the occurrences of neutron star superbursts resulting from accretion. Experimental challenges at these energies obstruct even a gross knowledge of these cross sections, thus also the possibility of a strong fusion hindrance was considered. This idea comes from the extension to light nuclei fusion of the low energy fusion cross section hindrance of medium and high mass ions, which is now established for these negative Q-value fusion reactions Ş. Mişicu and Esbensen (2006); Jiang et al. (2008). For lighter ion-ion reactions hindrance causes assumed are the incompressibility of nuclear matter and the Pauli principle. For these reasons, studies of the systematics of these reactions and reactions between nearby nuclei at sub-Coulomb energies are still undergoing. ^{12}C + ^{12}C is one of the most important reactions in nuclear astrophysics, due to the strong influence that carbon burning has on the fate of massive stars Chieffi et al. (2021) and super-bursts from accreting neutron stars Schatz et al. (2014).

According to present understanding, carbon burning occurs at temperatures of about 800 MK, corresponding to the reactions effectively occurring in the energy range E$_{c.m.}$ = 1.0 - 2.0 MeV, with sub-fb cross sections. Direct measurements, so far, reported results affected by high uncertainty down to about E$_{c.m.}$ = 2.2 MeV Becker et al. (1981); Barrón-Palos et al. (2006); Spillane et al. (2007); Jiang et al. (2018); Zickefoose et al. (2018); Fruet et al. (2020); Tan et al. (2020), with resonances adding extra uncertainties. Besides the extremely low cross section, environmental and beam induced background was the main limitation for direct measurements, the latter due to H, D and ^{13}C contaminations in carbon targets Becker et al. (1981); Barrón-Palos et al. (2006); Spillane et al. (2007); Jiang et al. (2018); Zickefoose et al. (2018); Fruet et al. (2020); Tan et al. (2020).

Multiple experimental efforts are focused on performing direct measurements of carbon fusion cross section and measurements with improved accuracy right inside the astrophysics region of interest of core carbon burning in heavy stars Fruet et al. (2020); Tan et al. (2020, 2024); Monpribat et al. (2022). The measurement setups are designed for reliable and enduring detection of the charged particles (alphas and protons) evaporated from the compound nucleus ^{24}Mg in coincidence with gammas from the de-excitation of the daughter nuclei (^{20}Ne, ^{23}Na) with efficient background suppression for the accurate determination of cross sections of 100 *nb* or below Heine et al. (2018, 2022). This necessitates measurements campaigns of typical several weeks with bombardment of the carbon targets with carbon beam of an intensity of up to 10 pμA. Under such high-duty conditions, accurate knowledge of the intact state of the target are indispensable Aguilera et al. (2006); Tan et al. (2024) and multiple characterization before, during and after beam exposure are combined during the measurements with STELLA (STELlar LAboratory) in order to guarantee accurate measurements Heine et al. (2018); Nippert et al. (2024), as it is shown in 1.1.1.

Also, LUNA collaboration proposed a new direct measurement at the deep underground Bellotti Ion Beam Facility (B-IBF) of LNGS, Italy. LUNA aims at measuring the cross sections of the ^{12}C(^{12}C,α)^{20}Ne and the ^{12}C(^{12}C,p)^{23}Na reactions by detecting γ-rays emitted in the de-excitation of the ^{23}Na and ^{20}Ne nuclei, produced in an excited state after the emission of a charged particle by the compound nucleus. This

approach would benefit the most from the deep underground location of the B-IBF, where cosmic rays are suppressed by six orders of magnitude, reducing to almost zero the high energy γ background and enabling the use of thicker lead shielding around the detector. The dynamic range of LUNA-MV 3.5 Singletron accelerator is 1-7 MeV, allowing to perform a comprehensive measurement of the $^{12}C + ^{12}C$ reaction cross section. Moreover the expected $^{12}C^+$ and $^{12}C^{++}$ beam intensities at the B-IBF are up to 150 μA Sen et al. (2019), which allows to achieve the proper sensitivity Piatti (2024), but still the target to be used is a crucial element for these measurements, as detailed in sec. 1.1.2.

Besides direct approaches, recently a measurement of the $^{12}C+^{12}C$ cross section was performed with Trojan Horse Method (THM), which is based on the transfer of a ^{12}C nucleus to ^{12}C in the three-body processes $^{12}C(^{14}N,\alpha^{20}N)^2H$ and $^{12}C(^{14}N,p^{23}Na)^2H$ in the quasi-free kinematic mechanism Tumino et al. (2018). The extracted astrophysical S-factor presents several resonances that enhances the reaction rate by a factor of up to one hundred, with significant impact on our present knowledge of the carbon burning.

The THM data do not suggest any hindrance effect and this is also what has been found on $^{12}C+^{13}C$ fusion by Zhang et al. (2020). More specifically, with respect to the ongoing hindrance-debate for low mass fusion reactions Montagnoli et al. (2020); Gharaei et al. (2021); Sargsyan et al. (2022), the results in Zhang et al. (2020) suggest that a maximum in the S-factor is not in fact present for the $^{12}C + ^{12}C$ reaction. Indeed, while $^{13}C + ^{12}C$ does not show a resonant behavior as $^{12}C + ^{12}C$, it was determined that it does indicate an upper limit for the resonant cross sections as well as a general trend for the behavior of the astrophysical S-factor Notani et al. (2012).

Moreover, a complementary study was done by the Nuclear Astrophysics Group (NAG) at "Horia Hulubei" National Institute for Physics and Nuclear Engineering (IFIN-HH) using the local 3 MV Tandetron and the activation method. The reaction was studied through the adjacent system $^{13}C + ^{12}C$. The proton evaporation channel produces the unstable ^{24}Na with a half-life of 15 hours and its deactivation could be measured inside the Slănic salt mine in an ultra-low background environment Tudor et al. (2020). This allowed for the determination of the fusion cross section at deep sub-barrier energies, with the goal of determining the low energy trend of the fusion cross section and of testing the hindrance hypothesis, that should be observed in all of the exit channels and in adjacent systems.

Similarly, in order to help the current understanding of fusion mechanisms at sub-Coulomb energies in low-mass ion-ion systems, the NAG group has continued to study similar reactions (see subsections 1.2 and 1.3). Because activation was found to be the most sensitive method, the reactions studied were chosen based on the activation channels produced as well as on the combination of beam intensities and targets available. Below we show the various targets that were produced and tested for these studies.

1.1 $^{12}C+^{12}C$

1.1.1 The STELLA rotating target system

The STELLA collaboration is engaging in direct carbon fusion measurements with an innovative rotating-target mechanism employing large thin self-supporting carbon foils Heine et al. (2018); Nippert et al. (2024). In this approach, the beam traverses the foil undergoing an energy loss of typically 100 keV, and subsequently its charge is determined in a separate beam dump (Faraday cup) for data normalization. The beam hits an outer trajectory of the target-foil surface (target frame diameter: 6.3 cm), that is spinning with of up to 1000 rpm and effectively cooling down by radiating when rotated out off the nominal beam spot position. During data taking periods, the intact status of the target foil is online monitored by the ratio of the counting rate of the beam dump to elastic beam-scattering observed with dedicated silicon detectors further away from the target.

The thickness of the target foils is obtained upon production by high-precision mass determination. These measurements are accompanied by samples of Raman-spectroscopy analysis of the carbon target foil material after beam exposure Fruet et al. (2020) and systematic thickness determination with an alpha-particle emitting source measuring the thickness dependent energy loss. To this purpose, the measurement station displayed in Figure 2 was developed in collaboration with the University of York. The device hosts an alpha emitter, a mobile target holder and a silicon detector. In a series of measurements alternating between points on and off area with beam exposure, the energy loss is determined and converted into the target thickness. Note that the beam spot forms a circular track on the STELLA targets from the rotating system. A measurement hence yields a sequence of eight data points along the outer radius of a target foil with an equal amount of reference points at the center to guarantee the accuracy of the method. A variety of such scans is presented in Figure 3

as a function of the angle along the beam track. Data follow a sine curve indicating a slight thickness gradient of the target foils (see Nippert et al. (2024) for details) and several target-foil patches are grouped by the color code. For the normalization of the $^{12}C+^{12}C$ measurements, the average target thickness, which is in good agreement with the thickness determination upon target production, is used. This routine improves the precision of the target thickness to better than 10% and furthermore excludes carbon built-up on the
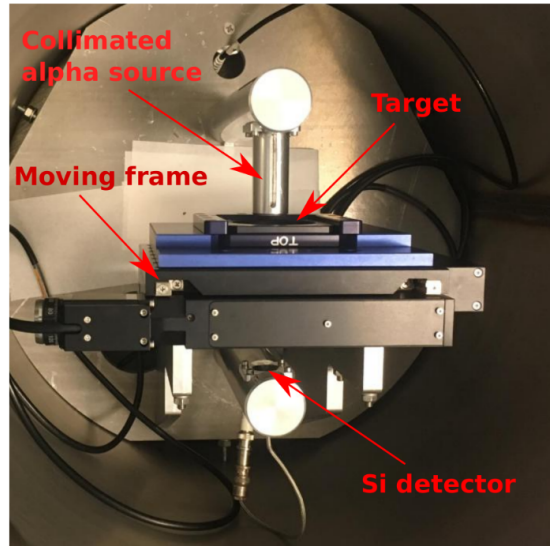
Figure 2. Photograph of the target foil measurement station for characterizing large thin carbon target foils at IPHC Strasbourg.

target Healy, M.J.F. (1997); Aguilera et al. (2006); Fruet et al. (2020) demonstrating the reliability and accuracy of the target foil normalization during the ^{12}C+^{12}C measurements with STELLA. Such routines are in high need, seen the challenges of exact target thickness determination in such experiments Tan et al. (2020, 2024).

1.1.2 Contaminants desorption with HEAT and the tests on carbon targets for the LUNA measure-ment

The presence of a strong beam induced background due to the interaction of the carbon beam with hydrogen and deuterium contamination inside the targets: ^{1}H(^{12}C,γ)^{13}N, ^{2}H(^{12}C,pγ)^{13}C and the two-step process ^{2}H(^{12}C, ^{2}H)^{12}C $\rightarrow$ ^{12}C(^{2}H,pγ)^{13}C hamper the cross section measurement at low energies Zickefoose et al. (2018); Morales-Gallegos et al. (2018); Spillane et al. (2007). In literature, irradiating the target for few minutes, heating it up to hundreds of Celsius degree, was reported as an efficient technique to reduce the hydrogen contamination Spillane et al. (2007). However beam heating lacks of reproducibility. Despite the thick target approach is favored over thin target, which suffer of C-buildup problem Becker et al. (1981), other technical difficulties arise, such effective cooling of the target and detectors closed by, radiated heat and deposition of carbon inducing structural changes in the target Spillane et al. (2007); Picollo et al. (2021).

The HEAT project (Figure 4) at the Laboratori Nazionali in Legnaro (LNL) of INFN, in Italy, aims at developing pure carbon targets for measurements of the cross section of the ^{12}C+^{12}C fusion reaction. The goal of the HEAT experiment is to establish a reproducible technique for hydrogen desorption from different types of carbon targets, to ideally decrease the hydrogen content at the level of a few ppm.

Targets investigated so far include natural graphite, HOPG and glassy carbon Depalo et al. (2021). The measurements confirm that HOPG is the graphite with the lowest content of hydrogen. In natural graphite, desorption levels as high as a factor of 3 have been observed (see Figure 5). Desorption tests on tantalum, one of the most common backing material for solid targets, have also been performed, and the setup could be used in the future for different applications.

HEAT studies for the amount of H and D contaminants were found to be relevant for the target choice of the ^{12}C+^{12}C cross section measurement planned by LUNA collaboration at the B-IBF at LNGS. Additionally, LUNA collaboration tested the different types of target stability under irradiation and their thermal behavior for a properly designed target holder. The first tests have been performed at the shallow underground facility of Felsenkeller. A 8.8 MeV beam of ^{12}C^{+++}, with intensity 2-5 pμA, was delivered to natural graphite, HOPG, glassy carbon and AXF and ZXF-type graphite from ENTEGRIS, as shown in Figure 6. These targets were selected because of either low H and H_2 content (HOPG), good thermal resistance (Glassy carbon and graphite) or conductivity (HOPG) and their nanostructure (AXF and ZXF-type graphite). From preliminary analysis the AXF and ZXF graphite proved to be the most stable in terms of thermal and structural behavior, and for this reason, they are good candidates for the LUNA measurement. Analysis is ongoing to check the contamination level in each different target as well as the
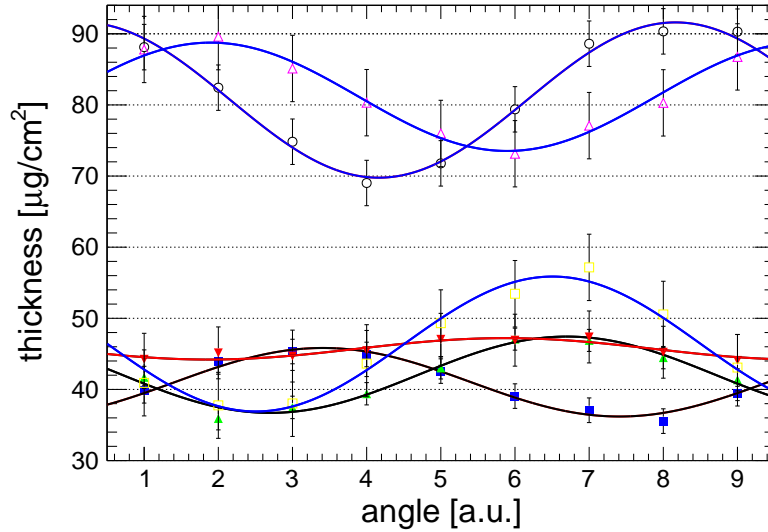
Figure 3. Sequences of target thickness determination measurements at IPHC Strasbourg for large thin carbon targets. Data are taken in iterative measurements on and off the irradiated target area and several target production patches are indicated by the color code of the fitting curves (see text for details).

beam induced degradation in each of them.

1.2 ^{12,13}C+^{16}O

As mentioned at the beginning of this section, fusion reactions between light ions, especially ^{12}C and ^{16}O, play an important role in stellar evolution and explosive nucleosynthesis. The reaction ^{12}C+^{16}O has been found to have a significant contribution in both the carbon and oxygen burning stages of stars Wiescher et al. (2012); Woosley et al. (1971). While ^{12}C+^{12}C is the main reaction during core and shell carbon burning, towards the end of this phase as ^{12}C nuclei are depleted, the abundance of ^{16}O becomes substantially higher as a result of the ^{12}C(α,γ)^{16}O Weaver and Woosley (1993); Buchmann (1996). A similar scenario occurs in oxygen burning, where the ^{16}O+^{16}O reaction is dominant. Here, as ^{16}O nuclei are depleted, the photodissociation of ^{16}O increases the abundance of ^{12}C nuclei leading to potential reaction with ^{16}O. In both cases, the competitiveness of the ^{12}C+^{16}O is enabled by the temperature and density increases, characteristic of late stage burning. It has also been shown in recent studies Martínez-Rodríguez et al. (2017) that this reaction can play an important role in the evolution of Type Ia supernovae, depending on the relevant fusion rates and environmental conditions.

It is, therefore, similarly important to perform studies of the sub-Coulomb barrier fusion cross section of the ^{12}C+^{16}O reaction. So far, in literature, most of the measurements that can be found for this reaction were performed in the 1970s Patterson et al. (1971); Christensen and Switkowski (1977); Čujec and Barnes (1976) with oxygen beams and natural carbon targets. However, they all stop at a center of mass energy of $\sim$4 MeV leading to the necessity of using extrapolation methods for lower energies. A more recent study was performed by Fang et al. Fang et al. (2017) using single and particle-γ coincidence techniques, which extended the known experimental range down to $\sim$3.6 MeV and hinted at the presence of the hindrance phenomenon. Even more recently, in Oliva et al. (2023) is reported the completion of an experiment at the Laboratori Nazionali del Sud, Italy, that used the indirect THM method to evaluate the ^{12}C(^{16}O,α)^{24}Mg and ^{12}C(^{16}O,p)^{27}Al reactions at astrophysical energies, but data analysis is still ongoing.

Because of the many open questions left by other studies, at IFIN-HH, the ^{12}C + ^{16}O reaction was studied through the neighboring reaction, ^{13}C + ^{16}O, using the very sensitive activation method in order to determine partial cross sections, and therefore the total fusion cross section. This reaction produces three radioactive isotopes, ^{28}Al (T$_{1/2}$ = 9.8 min), ^{27}Mg (T$_{1/2}$ = 2.24 min) and ^{24}Na (T$_{1/2}$ = 15 hours), and as such the focus was on measuring gamma decay spectra down to the lowest energies possible. Experimentally, this was approached in two ways: a ^{16}O beam on ^{13}C targets and a ^{13}C beam on ^{16}O targets.

1.2.1 ^{13}C targets

The first approach, as mentioned above, was to use an ^{16}O beam on a ^{13}C target. The oxygen beam was produced from NiO at energies E$_{lab}$=10-14.8 MeV with currents between 3 pμA and 240 pnA, respectively. Thin ^{13}C targets were prepared by deposition of ^{13}C (from powder with 99% purity) on Ta backing (a foil of 3 mg/cm^2 thickness) using the electron-gun method part of the TE18-High Vacuum Deposition

Figure 4. Picture of the HEAT setup installed at the AN2000 accelerator facility of Legnaro National Laboratories.
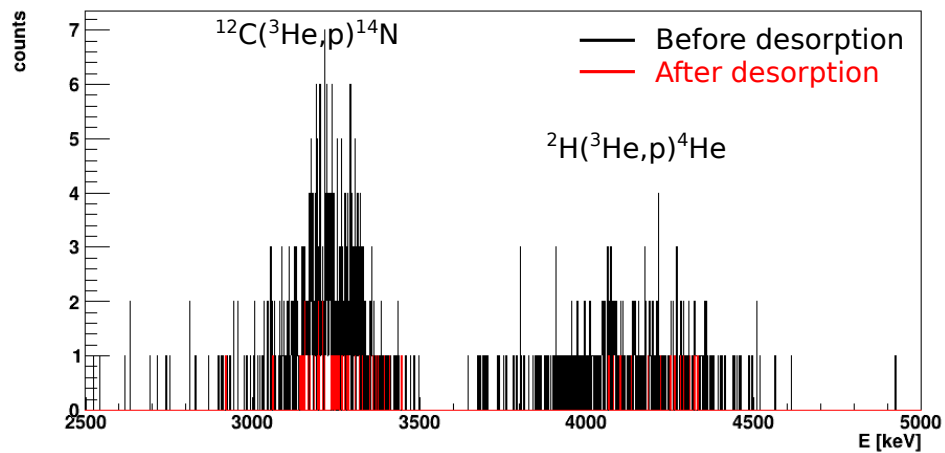
Figure 5. Natural graphite (0.95% nominal purity) spectra before and after a 1 MeV beam of ^{3}He.

System produced by Intercovamex company. Figure 7 shows a picture of one such target. The thickness of the deposited ^{13}C layer for each target was determined using the RBS technique, using a proton beam from the 3 MV Tandetron at IFIN-HH accelerator at energy of 2.5 MeV. An example of RBS spectrum is shown in Figure 8, showing the data (red circles) for the central spot of the target in Figure 7, as well as the simulation performed with SIMNRA 7.0 Mayer (1999) (blue line). The thickness of these targets was determined to be, on average, 170 nm (40 μg/cm^2). A visual assessment of the targets showed the presence of significant rugosities in the beam spot area, an effect that leads to thickness non-uniformity and uncertainties in cross section estimations.

Given the short half-lives of the unstable nuclei produced (^{27}Mg with $T_{1/2}$=9.8 min and ^{28}Al with $T_{1/2}$=2.2 min), the targets were used for repeated measurements of 30 - 60 minutes irradiation followed by 50 minutes decay measurements. The targets were assessed on a visual level after each irradiation and found to be deteriorating even when lower beam currents were used. Specifically, it was determined that the heat generated by the beam was causing the carbon layer to form bubbles, eventually leading to complete detachment (Figure 9).

It should be noted that the flange holding the target was cooled with a water-based system during irradiation, but it appears that it was insufficient. Post-irradiation Scanning Electron Microscopy (SEM) confirmed the absence of carbon in the beam spot (Figure 10), leaving only the Ta backing with flakes of ^{13}C on the border.

Given these test results and that the NAG group's interest is in very low energies and low cross sections
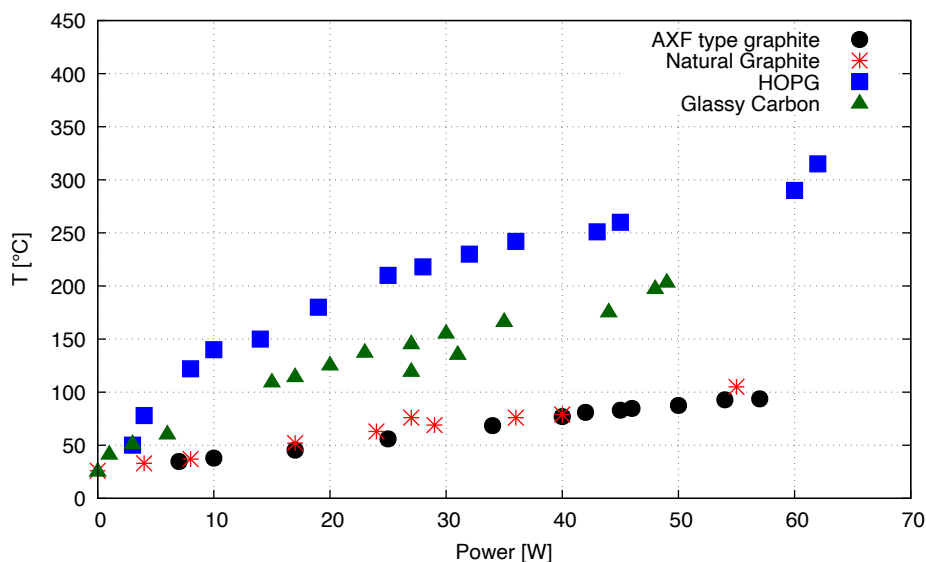
Figure 6. AXF ENTEGRIS graphite (black circles), Natural graphite (red stars), HOPG (blue squares) and glassy carbon (green triangles) temperature of the beam spot. The ENTEGRIS graphite shows the best thermal conductivity and after long irradiation (up to 3 C) showed the best endurance. HOPG and Glassy C showed, indeed, a swelling beamspot and a crack respectively.

measurements, where high beam currents are paramount, it was decided that such thin targets could not be used for these purposes.

1.2.2 Oxygen targets

The second approach was to use a ^{13}C beam on an ^{16}O target. The carbon beam was produced at different laboratory energies between 8 and 15 MeV with currents between 3 pμA and 200 pnA, respectively. Several oxide compounds were tested, chosen primarily based on two criteria: the Z of the compound partner (higher means higher Coulomb barrier, therefore a lower probability to induce a contaminant reaction with the beam) and the number of oxygen atoms in the compound.

(a) Cerium dioxide (CeO$_2$) The first compound that was tested was cerium (IV) oxide. Targets were prepared from CeO$_2$ powder using the tablet pressing method. The powder was pressed into pellets by applying a load of 25 ton. The diameter of the pellets was set at 2 cm or less in order to fit inside the target holder, but different thicknesses were attempted: 0.8 g/cm^2 and 1 g/cm^2. It was found that the targets could not be made any thinner than 0.75 g/cm^2, as they became too fragile to handle and crumbled immediately.

In order to provide support and easier handling, the pellets were attached to aluminum backing in the shape of discs ($\sim$1 mm thick). The targets were irradiated on average for 60 minutes and were affected on various levels by the beam, depending on the current. Figure 11 shows the beam spot of a CeO$_2$ target (0.8 g/cm^2) after 40 min of irradiation with ^{13}C at 10.8 MeV and a current of $\sim$80 pnA ($\sim$1 mC beam charge). Similarly, Figure 12 shows a different target (0.8 g/cm^2) after a slightly longer irradiation (60 minutes) but with a beam current of $\sim$1 pμA ($\sim$10 mC beam charge).

This was considered a better option than the previously described ^{13}C targets and as such the CeO$_2$ pellets were used for the measurement of the ^{13}C + ^{16}O cross section, for a range of energies E$_{lab}$ = 8-15 MeV, in steps of 0.4 MeV. Figure 13 shows a typical gamma decay spectrum obtained for this measurement with the target in Figure 12 at a beam energy of 10 MeV. Two gamma peaks of interest were clearly observed at the expected positions in the spectrum, E$_\gamma$ = 1368 keV from ^{24}Na and E$_\gamma$ = 1779 keV from ^{28}Al, as shown by the red arrows. The remaining active channel of the three produced in this reaction was not observed at this energy, as its cross section is significantly lower comparatively. An issue that was noticed immediately was that irradiations could not begin at the highest current available because vacuum would break immediately. Instead, a beam intensity of $\sim$50 pnA was used at the beginning and then increased slowly over the duration of the irradiation (Figure 14). Given the short half-lives of the nuclei of interest, it was necessary for this variation in beam current to be recorded and corrected for in the final yield calculations.

Over the duration of the experiment, it was determined that the targets could be irradiated a maximum

Figure 7. Picture of a ^{13}C targets made by deposition on Ta backing.
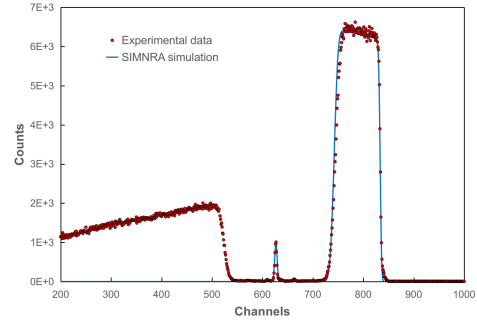
Figure 8. RBS spectrum for the target on the left, showing the small peak corresponding to ^{13}C and the larger one denoting the Ta backing. The slight disagreement between the simulation (blue line) and the experimental data (red dots) is due to the presence of rugosities on the surface (as can also be seen in Figure 7).
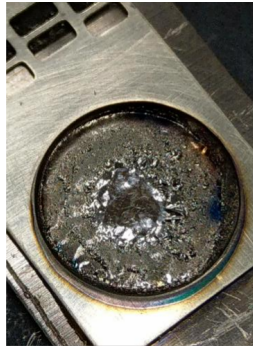
Figure 9. Picture of one ^{13}C target after irradiation with beam currents of ∼1 pμA.
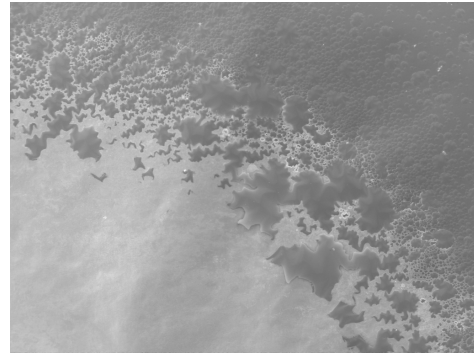
Figure 10. Picture taken of target in Figure 9 with SEM at 100x magnification, showing the transition between the beam spot (polished surface) and the rest of the target surface (rough surface).

of 3 times at the highest currents before becoming unusable and up to 5 times at intensities on the order of ∼250 pnA. We suspect that the damage sustained by the pellets was due to the heat produced because of the high beam intensity, even though the target holder was equipped with a water-cooling system. It was concluded that the best option for such targets is for them to be used for a single measurement/irradiation, upon the availability of the material. Unfortunately, for the study of ^{13}C + ^{16}O, the limitation on irradiation time led to an inability in studying the longer-lived activation channel (^{24}Na, $T_{1/2}$ = 15 hours) at lower energies and cross sections.

(b) Tantalum pentoxide (Ta$_2$O$_5$)   Targets of Ta$_2$O$_5$ prepared at Laboratori Nazionali del Gran Sasso of INFN, Italy , by anodization of tantalum backings in ultrapure water, were also used and tested. The details of this technique can be found in the work reported in Caciolli et al. (2012). Two targets with two different thickness of the Ta$_2$O$_5$ layer (∼171 nm and ∼438 nm) were prepared, the latter is shown in Figure 15.

Before the activation test, both targets underwent RBS measurements to verify stoichiometry and determine the thickness of the Ta$_2$O$_5$ layer as well as its uniformity. The measurements were carried out at IFIN-HH with the 3 MV Tandetron using a ^{4}He beam (∼1 mm^2 spot size) and E$_{lab}$ = 2.00 and 3.01 MeV. An example of the scattered α spectra obtained with a silicon detector at 165° can be seen in Figure 16, showing the data (red circles) for the central spot of the target in Figure 15, as well as the simulation performed with SIMNRA 7.0 (black line). The continuous 'background' indicates the Ta backing, whereas the 'shoulder' on the right shows the Ta$_2$O$_5$ layer. Both targets were found to have a uniform layer of Ta$_2$O$_5$ and the expected stoichiometry of ∼0.4. However, due to the thinner backing, the target in Figure

Figure 11. CeO$_2$ target seen with microscope at 8x magnification showing damage after 1 mC irradiation.
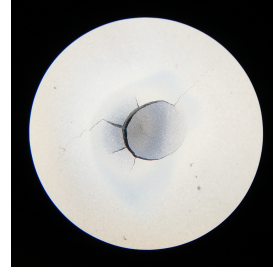
Figure 12. CeO$_2$ target seen with microscope at 8x magnification showing damage after 10 mC irradiation.
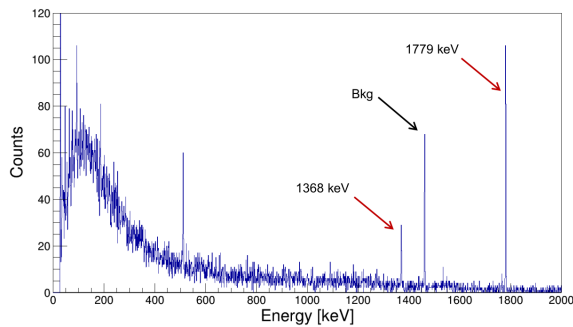
Figure 13. Gamma decay spectrum after irradiation of CeO$_2$ target with ^{13}C at 10 MeV energy and $\sim$1 pμA beam intensity. Red arrows indicate the peaks of interest. The black arrow indicates a background peak.
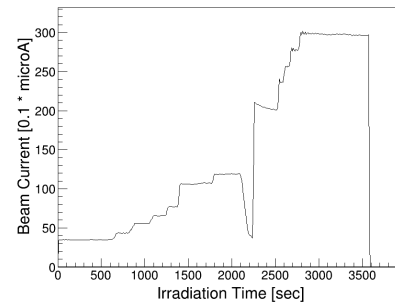
Figure 14. Beam current variation with irradiation time. X-axis shows the time in seconds. Y-axis shows the beam intensity in units of 0.1*μA.

15 experienced rugosities in transport, which can be seen in the slight disagreement between experimental data and simulation. The layer thickness for each target was found to be $\sim$171 nm and $\sim$438 nm.

The activation test was done with a ^{13}C beam and a focus on the longer lived ^{24}Na + pα channel (T$_{1/2}$[^{24}Na] = 15 h). The goal was to determine the sturdiness of the targets, specifically the oxide layer, under high beam currents and longer irradiations (relative to the previous targets tested). Due to the limited amount of beamtime available, it was not possible to actually test 24-hour long irradiations, which would be necessary at the energies of interest (below E$_{lab}$=7 MeV). The targets were irradiated with beams at different energies and with different total beam charge (approximately 30 mC and 70 mC, respectively). Figure 17 shows an example of a gamma decay spectrum obtained from the 438 nm thick Ta$_2$O$_5$ target. The gamma peak marked in red is at E$_\gamma$ = 1368 keV and results from the decay of ^{24}Na, one of the active channel of interest (-p) for the fusion cross section determination.

The targets held well under vacuum and were easy to handle, which was an improvement over the CeO$_2$ pellets that were previously used. After decay measurements, the RBS test was repeated to determine how much deterioration the Ta$_2$O$_5$ layer suffered due to the irradiation. Figure 18 shows a comparison between the α spectra pre and post irradiation for the thicker target. The x-axis has been zoomed around the Ta$_2$O$_5$ 'shoulder' to emphasize the deterioration. Unfortunately, as it can be seen from the figure, the deterioration was complete in the beam spot region. Furthermore, we cannot estimate at which point during the irradiation the Ta$_2$O$_5$ layer disappears, thus we could not correctly determine any of the quantities of astrophysical interest, such as yield or cross section. The difference is that for this ion irradiation case, the energy loss in the oxide target is much higher than that of the proton reactions studied at LUNA.

To conclude, Figure 19 shows a comparison between gamma decay spectra obtained with the three types of targets described in this subsection. All irradiations were done at similar center-of-mass energies and the spectra were recorded for 5 minutes each. The blue line indicates data obtained with a Ta$_2$O$_5$ target, red shows data from a CeO$_2$ pellet and black represents a ^{13}C target. Two energies are indicated with dashed lines, corresponding to gammas from 2 activation channels: 1368 keV from ^{24}Na, and the 1779 keV peak from ^{28}Al. The red peak at 1779 keV in Figure 19 suggests that, although difficult to handle, CeO$_2$ pellets can be used with currents lower than 1.5 pμA and irradiation times smaller than 1.5 h. This means they do not allow for the study of the longer-lived activation channel but can be used successfully to

Figure 15. Photograph of the Ta_2O_5 target with layer thickness of ~438 nm.
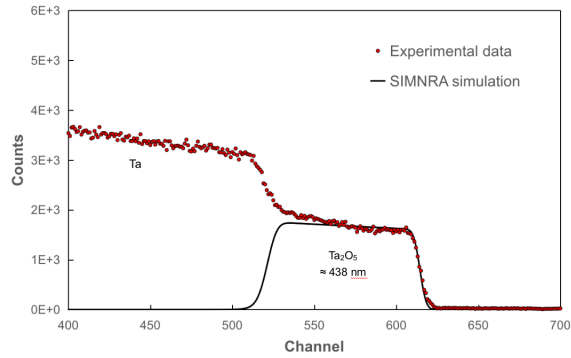
Figure 16. RBS spectrum from the central spot of the target in Figure 15. The simulated tantalum oxide layer thickness (black line) does not agree perfectly with the experimental data (red dots), presumably due to the presence of rugosities on the surface (as can also be seen in Figure 15).
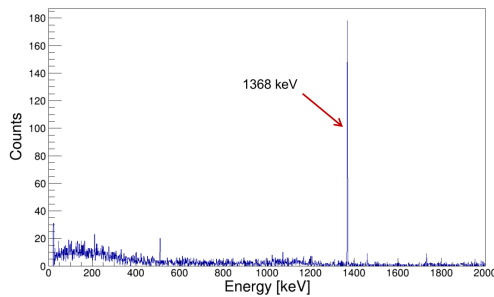
Figure 17. Gamma decay spectrum after irradiation with ^{13}C at 8 MeV, recorded for ~3.5 hours. The red arrow indicates the peak from ^{24}Na, at 1368 keV.
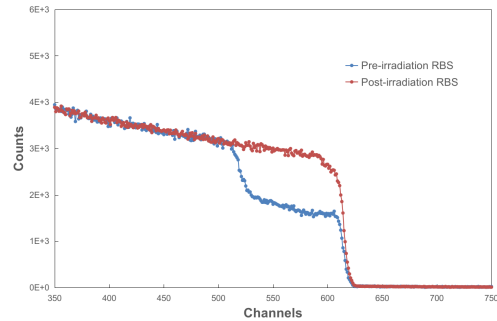
Figure 18. Comparison RBS spectrum from the center of the beam-spot showing the complete degradation of the Ta_2O_5 layer. Blue line indicates pre-irradiation data. Red line indicates post-irradiation data.

measure short-lived nuclei like ^{28}Al. ^{13}C and Ta_2O_5 are much better in terms of handling but require a method to monitor the target deterioration during irradiation, as well as post-measurement RBS in order to account for the loss of material. Lastly, in terms of amount of target atoms provided, the anodized Ta_2O_5 targets appear to contain the most among the three, therefore providing the best statistics. This can be seen in the presence of the blue peak in Figure 19 from ^{24}Na and the absence of any overlapping red ones in the CeO_2.

These tests were crucial to decide for the CeO_2 targets in the study the $^{13}C+^{16}O$ reaction with the thick target activation method at IFIN-HH. Figure 20 shows partial results for the experimental cross sections for the two short-lived activation channels that could be measured, $^{28}Al+p$ (black points) and $^{27}Mg+2p$ (blue points). Comparison with previous studies is also shown with red points (from Ref. Dasmahapatra et al. (1991)), but only for the p-channel as they did not have measurements for the second one. Despite the limitations present in using the pressed cerium oxide pellets, it was possible to extend the known cross sections towards lower energies. Further measurements are planned at IFIN to extend this range towards lower energy, in order to support the theoretical studies of fusion mechanisms.

1.3 $^{12,13}C+^{19}F$

As part of the ion-ion fusion reactions program, the NAG group at IFIN-HH also intends to study the fusion reactions $^{12,13}C + ^{19}F$ at energies below the Coulomb barrier. They fall in the mass region considered "light-light" for fusion systems and despite their potential for fusion mechanisms studies, or to resolve the matter of the proposed hindrance mechanism, these reactions have not been studied in depth before. The most recent study is presented in Gaedke et al. (1968) and provides yields and cross section results for the two main activation channels that are produced in the reaction $^{nat}C + ^{19}F$, obtained for the purpose of estimating possible contamination in their other data of interest. The energy range only reaches as
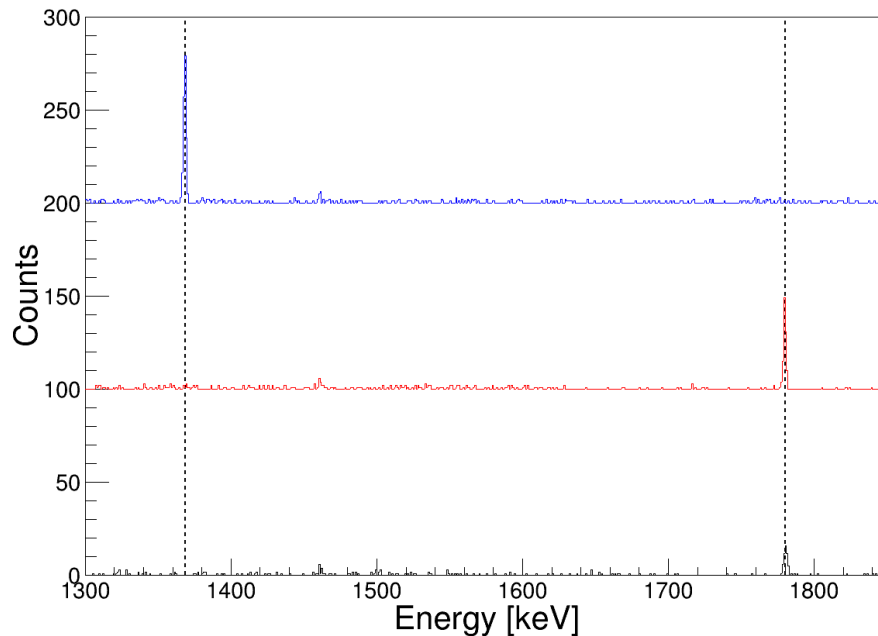
Figure 19. Comparison between gamma decay spectra obtained with the three types of targets described. Blue (top) indicates Ta_2O_5, red (middle) shows CeO_2 and black (bottom) is ^{13}C. X-axis is zoomed around the two energies of interest which are shown with dashed lines. The spectra have been offset on the vertical axis for easier visibility. All irradiations were done at similar center of mass energies and the spectra were recorded for 5 minutes each.

low as $E_{CM} = \sim 7$ MeV and it is not low enough to determine the presence or absence of the hindrance phenomenon, although it falls under the Coulomb barrier for this system.

Given that ^{13}C targets have already been tested, as shown in the previous section, the focus of the tests for this reaction was on determining the suitability of two types of fluoride materials: (a) LiF and (b) BaF_2. Unfortunately, due to time constraints on the beam availability it was not possible to perform extensive testing, as above.

(a) Lithium Fluoride (LiF)   The first compound that was assessed was lithium fluoride. Targets were made from LiF powder pressed into pellets at 10 Ton. The diameter of the pellets was 1.3 cm and they were also placed on thin aluminum disks for easier handling. One issue that was immediately apparent was that due to the hygroscopic nature of the material, they outgassed more strongly and it took longer to reach the intended beam current during irradiation, even for relatively low intensities. A second consequence of that was the presence of contaminant reactions on hydrogen and oxygen. In particular, reactions on oxygen produce similar gamma peaks to those of interest from fluorine.

A LiF target was irradiated for 1.5 h with a ^{13}C beam at laboratory energy 18 MeV and intensity ~ 50 pnA (~ 1.3 mC). A visual assessment with an 8x microscope showed a highly visible beam spot but no surface deterioration. The pellet also handled transportation from the beamline setup to the decay station without suffering damage. However, the deactivation spectra showed large background from decaying nuclides produced in the reaction on lithium (Figure 22, blue line). For the purpose of measuring cross sections at low energies where the activation method is more sensitive than prompt measurements, having an increased background is not desirable and therefore, this type of target was found to be unsuited for these experiments.

(b) Barium Fluoride (BaF_2)   The second compound that was tested was barium fluoride. The targets were made from BaF_2 powder, also pressed into pellets at 10 Ton pressure. Barium has a much higher proton number and as such, the issue of contamination in the spectra was eliminated. The diameter of the pellets was also 1.3 cm and they were placed on rectangular aluminum backings for easier handling. The main issue here was that BaF_2 powder does not compact well and the pellets were more fragile to handle than the LiF ones, so that some of them broke just handling. It is possible that a larger diameter for the pellets (which would allow a maximum pressure of 25 Ton to be used) will make them sturdier and it is an option to be tested in the future. A BaF_2 target was irradiated with the same ^{13}C beam and under similar parameters for consistency.
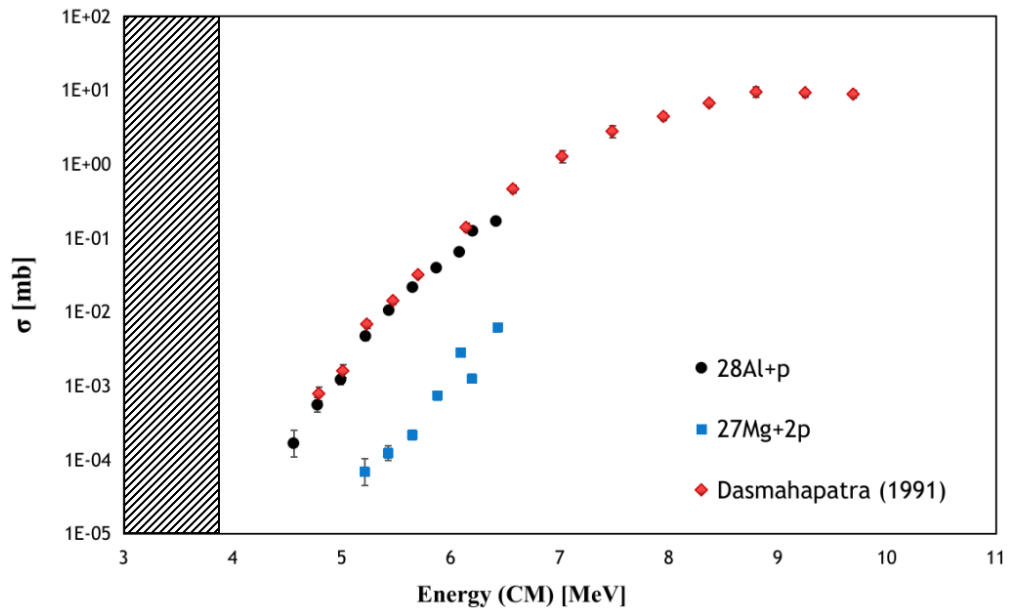
Figure 20. Experimental cross sections as a function of center of mass energy for the two short-lived active channels measured, $^{13}C+^{16}O \to {}^{28}Al+p$ and $^{13}C+^{16}O \to {}^{27}Mg+2p$. Error bars indicate statistical errors and are too small to be seen on the plot at higher energies. Red points indicate result from previous literature, Ref Dasmahapatra et al. (1991), for this reaction and respective channels. The hatched region shows the Gamow window for this reaction, estimated at $T_9 = 1K$.

Figure 21 shows a comparison between the prompt gamma spectra obtained with the two types of targets, the blue line representing LiF and red showing BaF_2. The most significant difference between them comes from the better statistics due to the increased stoichiometry of fluorine in BaF_2. Similarly, Figure 22 shows a comparison between the decay gamma spectra from the two targets (blue shows LiF, red shows BaF_2). As mentioned, with BaF_2 the peak-to-background ratio is much better compared to LiF, where lithium produces strong contaminant reactions. In conclusion, BaF_2 is the preferred option between the two and can be successfully used for the future measurements of $^{12,13}C+^{19}F$ that do not require beam currents higher than 0.5-1 pμA.
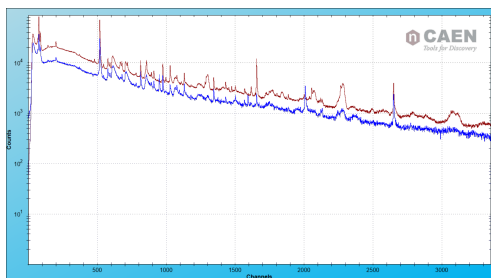
Figure 21. Prompt gamma spectra comparison between the two types of targets. Blue indicates LiF, while red indicates BaF_2. Both spectra were corrected for dead time and normalized to beam charge.
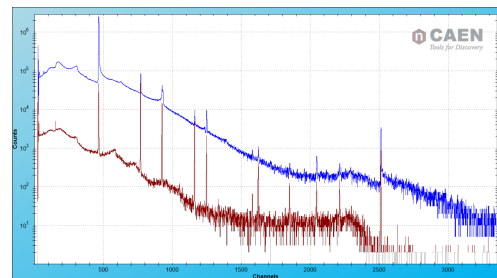
Figure 22. Decay gamma spectra comparison between the two types of targets. Blue indicates LiF, while red indicates BaF_2. Both spectra were recorded in 10 minutes and corrected for dead time.

2 HIGHLY ENRICHED FLUORINE TARGET FOR PHYSICS BEYOND THE STANDARD MODEL

Highly enriched fluorine targets have also been tried at Physical Chemistry Techniques Department of Laboratori Nazionali del Sud (LNS) of INFN in Catania, Italy.

These targets will be used also for the NEW JEDI experiment Bastin et al. (2023), which aims to explore potential physics beyond the standard model and in particular is devoted to the X17 boson search through the study of ^8Be level decay, populated via ^7Li+p, where LiF targets are being used. As usual when

the desired element (lithium) is not the only one in the target, to retrieve its contribution, highly enriched targets of the other elements present in the target (fluorine) are needed to determine the background produced.

CaF$_2$ targets   CaF$_2$ was chosen as a first attempt to produce targets with high fluorine content (usually in the form of salt). The PVD (Physical Vapor Deposition) deposition technique was used as a vacuum evaporation technique. The salt was deposited on amorphous graphite thin layers, 30 μg/cm^2 thick. It is worth noticing here that heating the sample to 180° was necessary before the salt evaporation, to remove the absorbed water by this very hygroscopic salt. Therefore, in high vacuum conditions, the salt placed inside the evaporator sublimates when heated. To control the evaporation process, a quartz microbalance was used, measuring the speed of the deposited salt as a function of time. To have further feedback of the target thickness, the α-particles scanning system was used, returning the value of 150 μg/cm^2.

PTFE targets   To overcome the important issues related to the salt hygroscopicity, looking for an easy to use and handle target, among the other investigated materials, a good choice has turned to be polytetrafluoroethylene PTFE, $-(F_2C-CF_2)n-$, also known as teflon. It is a plastic polymer with a large amount of fluorine ($\frac{C}{F}=\frac{2}{4}$) and density of 2.2 g/cm^3. The technique chosen was cold lamination. Even though teflon is a plastic material, at each lamination step the two rollers distance was reduced of 1/6 of a millimeter, to thin it optimally. The thickness of three teflon targets obtained was measured with the automatic α scanning machine, measuring the energy loss in the film of the α particles coming from ^{241}Am decay. Results are listed in Table 1, with the mean value obtained and their standard deviation (STD).

Table 1. Characterization of the new teflon target produced.

sample	Measure	ΔE [keV]	Thickness [μg/cm^2]
DP490	1	708.47	1051
	2	724.02	1074
	3	714.80	1061
	mean	715.76	1062
	STD	7.82	12
DP491	1	850.37	1262
	2	852.57	1265
	3	843.90	1252
	mean	848.95	1260
	STD	4.51	7
DP492	1	786.19	1167
	2	792.34	1176
	3	786.34	1167
	mean	788.29	1170
	STD	3.51	5

During the NEW JEDI experiment commissioning at UJF Nuclear Physics Institute (NPI) at Řež (Prague - Czeck Republic), those targets were tested under proton beam (Figure 23), where they proved to resist up to 200 nA of beam current, then underwent a quick deterioration.

In the commissioning period of NEW JEDI experiment, also the fluorine targets were tested. In Figure 24 the yields registered by one of the detectors are shown, normalized to one peak located at 2.6 MeV. These test were made with a proton beam of 1.070 MeV on 154 μg/cm^2 LiF target with a 40 μg/cm^2 C backing (pink line), a 40μg/cm^2 C target (black line), a 153 μg/cm^2 CaF$_2$ target with a 34 μg/cm^2 C backing (red line) and 1061 μg/cm^2 PTFE target (green line). Results from carbon and fluorine targets will be used for the background subtraction.

3 NUCLEOSYNTHESIS VIA S-PROCESS AND α-INDUCED REACTIONS

In recent times, nuclear astrophysicists have directed their attention toward cross sections pertinent to the s-process, taking into account the possibility that r-process abundances can be inferred from those of the s-process. The s-process nucleosynthesis follows a trajectory that meanders along the valley of β-stability, in proximity to the strongly bound isotopes of a given mass number A. The primary focus for slow neutron captures lies in the final Asymptotic Giant Branch (AGB) phase of low- and intermediate-mass stars Spartà et al. (2022). Stars with a mass up to 3 M$_\odot$ are, in fact, responsible for generating the main component of the s-process (i.e., nuclei ranging from Sr to Bi). The primary neutron source is known to be the

Figure 23. PTFE target tested with a Cyclotron proton beam of NPI of UJF.
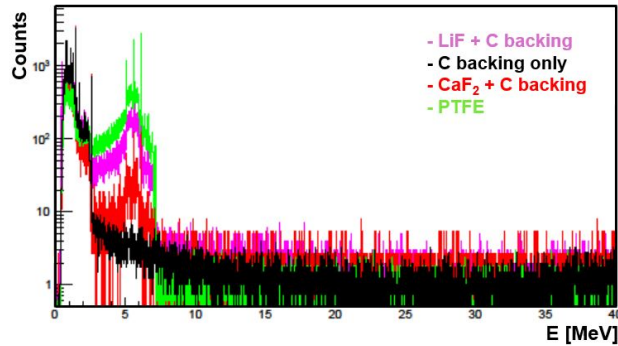
Figure 24. Yields from one detector of the NEW JEDI experiment obtained by a 1.070 MeV proton beam on different targets. Pink line is for a 154 μg/cm^2 LiF target with a 40 μg/cm^2 C backing. Black line for a 40μg/cm^2 C target. Red line for a 153 μg/cm^2 CaF$_2$ target with a 34 μg/cm^2 C backing. Green line for a 1061 μg/cm^2 PTFE target.

^{13}C(α,n)^{16}O reaction Busso et al. (1999). Operating at typical energies of 8 keV under radiative conditions, this reaction provides a neutron density of about $10^{6 \div 7}$ n/cm^3 Gallino et al. (1988) Iliadis et al. (2010).

A pivotal role in the s-process is played by the ^{22}Ne(α,n)^{25}Mg reaction, the primary neutron producer for its weak component (60<A<90) in massive stars, influencing all the late stages of stellar evolution until their demise. Despite the significance of this reaction, three orders of magnitude discrepancies persist in the cross section data within the energy range relevant for astrophysics (E$_{cm}$=300-900 keV), rendering such data essentially unusable for astrophysical purposes Longland et al. (2012); Adsley et al. (2021); Wiescher et al. (2023).

The trend of the excitation function measured so far indicates a steep drop in the yield, allowing for the provision of only upper limits to the cross section, even at center-of-mass energies around 800 keV, which is at the edge of the region of interest. A comprehensive overview of the current state of the field can be found in Jaeger et al. (2001). Direct measurements at such low energies are extremely challenging due to the exponential Coulomb damping (the Coulomb barrier is located at 3.5 MeV) of the cross section, reducing values to less than 1 μb and essentially pushing the signal-to-noise ratio to zero.

For this reasons, LUNA collaboration is working on a direct measurement of both the ^{22}Ne(α,n)^{25}Mg and the competitor ^{22}Ne(α,γ)^{26}Mg reaction cross sections at the B-IBF, exploiting the high intensity beam of LUNA-MV accelerator Sen et al. (2019), the ultra-low background, an extended ^{22}Ne gas target and a properly designed detector array Ananna et al. (2024, 2022); Mercogliano et al. (2024). Nonetheless, indirect measurements, such as capture and transfer reactions Jaeger et al. (2001), are necessary at low energy to provide resonance parameters, such as spectroscopic factors, for use in the calculation of the reaction rate. In this context, a recent paper Adsley et al. (2021) recalculated the reaction rates of ^{22}Ne(α,n)^{25}Mg and its competitor ^{22}Ne(α,γ)^{26}Mg, updating energies and spin-parities of all the ^{26}Mg

levels, with a particular focus on the results in Jayatissa et al. (2020), obtained through ^{22}Ne(^{6}Li,d)^{26}Mg and ^{22}Ne(^{7}Li,t)^{26}Mg transfer reactions. This leads to a better agreement of Ba and Zr isotopic ratios with data from presolar SiC grains. Nevertheless, the results reported in Adsley et al. (2021) and Jayatissa et al. (2020) suggest the need for further measurements, particularly focusing on the excitation function trend, to also account for levels interference in the evaluation of the reaction rate.

To deal with this, a possible solution is a new measurement of the ^{22}Ne(α,n)^{25}Mg with the indirect Trojan Horse Method (THM) Spitaleri et al. (2019); Tumino et al. (2021, 2025), using a ^{26}Mg beam as a ^{22}Ne inducer, the two-body reaction of interest being half of the energy shell. A sketch of the three-body reaction to measure to get the ^{22}Ne(α,n)^{25}Mg cross section at very low energies, is represented in Figure 25. THM results will be the better the lower the energy reached by LUNA measurement, because of the normalization needed by the method itself.
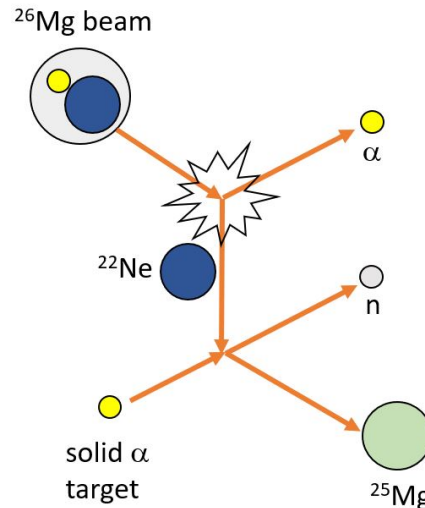
Figure 25. Sketch of a possible reaction to measure to get the ^{22}Ne(α,n)^{25}Mg cross section with the THM, taking advantage of the solid helium targets to be produced at LNS-INFN.

The use of solid α-targets is conditional to keep the low energy and angular spread needed by the THM to be used. Thus, noble elements solid targets are the next years challenge, that will be attempt at LNS of INFN in Catania, coupling the local Tandem pre-acceleration system and an ECR source who can provide also noble elements, with the idea to implant He and Ne into a host material, being impossible for them to create solid compounds, and then to test them to follow their stability under beam bombardment.

SUMMARY AND PERSPECTIVES

Substantial progresses in target preparation protocols at the STAR members laboratories are presented, in the framework of the ChETEC-INFRA project. In particular, pure and stable ^{19}F targets to match new experimental needs of nuclear astrophysics experiments, came out from investigations on new materials and protocols carried out both at IFIN-HH and LNS-INFN. At IFIN-HH also new ^{16}O and ^{13}C targets have been produced and tested for the study of the hindrance effect in light ion fusion at sub-barrier energies. Results shown claim for continuing the testing under beam bombardment of fluorine targets at IFIN-HH and the search for new and more resistant compounds for oxygen targets. Moreover, huge efforts have been dedicated in the research of ^{12}C targets to improve experimental chances to measure the fusion $^{12}C + ^{12}C$ reactions, critical to understand massive star evolution, as done by the STELLA collaboration. Tests of target stability under high intensity beam irradiation at Felsenkeller and H and D desorption from ^{12}C targets of the HEAT project, aim at suitable targets for the $^{12}C + ^{12}C$ cross section measurement planned by LUNA collaboration. Noble elements solid targets is the next years challenge, that for example will disclose the feasibility of an indirect measurements with THM of the ^{22}Ne(α,n)^{25}Mg cross section in the relevant energy region for astrophysics and, thus, to fix s-process models weaknesses.

For the first time, European target laboratories have been gathered in a context where they can learn from mutual experiences and cooperate. However, more than this, the whole European nuclear astrophysics community has shed light on the key role of the targets in the experiments. The problems in measuring cross sections coming from target non-uniformity effect, low resistance to intense beam currents and presence of contaminants, still require to continue these devoted studies by the STAR.

Thus, rather than the single laboratory improvement, the outlook for the future the possibility to improve together to meet the challenges of experimental requirements. This will be crucial for the step forward needed in nuclear astrophysics for the understanding of C-burning and the s-process.

FUNDING

REFERENCES

Adsley, P. et al. (2021). Reevaluation of the ^{22}Ne(α,γ)^{26}Mg and ^{22}Ne(α,n)^{25}Mg reaction rates. *Physical Review C*, 103(015805).

Aguilera, E. et al. (2006). Carbon buildup monitoring using RBS: Correlation with secondary electrons. *Nuclear Instruments and Methods in Physics Research B*, 244:427–435.

Ananna, C. et al. (2022). The shades neutron detection array. In *European Physical Journal Web of Conferences*, volume 260 of *European Physical Journal Web of Conferences*, page 11043.

Ananna, C. et al. (2024). Intrinsic background of EJ-309 liquid scintillator detectors. *Nuclear Instruments and Methods in Physics Research A*, 1060:169036.

Barrón-Palos, L. et al. (2006). Absolute cross sections measurement for the ^{12}C+^{12}C system at astrophysically relevant energies. *nphysa*, 779:318–332.

Bastin, B. et al. (2023). Investigation of a light dark boson existence: The new jedi project, Proc. of the 11th European Summer School on Experimental Nuclear Astrophysics. *European Physical Journal Web of Conference*, 275.

Becker, H. . et al. (1981). The ^{12}C+^{12}C reaction at subcoulomb energies. ii. *Zeitschrift fur Physik A Hadrons and Nuclei*, 303:305–312.

Buchmann, L. (1996). New Stellar Reaction Rate for ^{12}C(α, γ)^{16}O. *Astrophysical Journal Letters*, 468:L127.

Busso, M. et al. (1999). Nucleosynthesis in asymptotic giant branch stars: Relevance for galactic enrichment and solar system formation. *Annual Review of Astronomy and Astrophysics*, 37(1):239–309.

Caciolli, A. et al. (2012). Preparation and characterisation of isotopically enriched Ta$_2$O$_5$ targets for nuclear astrophysics studies. *The European Physical Journal A*, 48(144).

Chieffi, A. et al. (2021). Impact of the new measurement of the ^{12}C+^{12}C fusion cross section on the final compactness of massive stars. *The Astrophysical Journal*, 916(79).

Christensen, P. and Switkowski, Z. (1977). IWB analysis of scattering and fusion cross sections for the ^{12}C+^{12}C, ^{13}C+^{16}O and ^{16}O+^{16}O reactions for energies near and below the Coulomb barrier. *Nuclear Physics A*, 280(1):205–216.

Ciani, G. et al. (2021). Direct measurement of the ^{13}C(α,n)^{16}O cross section into the s-process gamow peak. *Physical Review Letters*, 127(15):152701.

Ş. Mişicu and Esbensen, H. (2006). Hindrance of heavy-ion fusion due to nuclear incompressibility. *Physical Review Letters*, 96(112701).

Čujec, B. and Barnes, C. (1976). Total reaction cross section for ^{12}C+^{16}O below the Coulomb barrier. *Nuclear Physics A*, 266(2):461–493.

Dasmahapatra, B. et al. (1991). Fusion cross sections for ^{12}C+^{12}C, ^{12}C+^{13}C and ^{13}C+^{13}C at low energies. *Nuclear Physics A*, 526(2):395–406.

Depalo, R. et al. (2021). The heat project: study of hydrogen desorption from carbon targets. *INFN-LNL Report*, 262:97–98.

Drotleff, H. et al. (1993). Reaction rates of the s-process neutron sources ^{22}Ne(α,n)^{25}Mg and ^{13}C(α,n)^{16}O. *The Astrophysical Journal*, 414:735–739.

Fang, X. et al. (2017). Experimental measurement of ^{12}C+^{16}O fusion at stellar energies. *Physical Review C*, 96(4):045804.

Fruet, G. et al. (2020). Advances in the direct study of carbon burning in massive stars. *Physics Review Letters*, 124(19):192701.

Gaedke, R. et al. (1968). Cross-section measurements for the nucleon-transfer reactions ^{10}B(^{19}F,^{18}F)^{11}B and ^{10}B(^{19}F,^{18}O)^{11}C. *Physical Review*, 167(957).

Gallino, R. et al. (1988). On the role of low mass asymptotic giant branch stars in producing a solar system distribution of s-process isotopes. *The Astrophysical Journal Letters*, 334:L45.

Gao, B. et al. (2022). Deep underground laboratory measurement of ^{13}C(α,n)^{16}O in the gamow windows of the s and i processes. *Physical Review Letters*, 129(13):132701.

Gharaei, R. et al. (2021). Survey of deep sub-barrier heavy-ion fusion hindrance phenomenon for positive and negative q-value systems using the proximity-type potential. *Chinese Physics C*, 45(124101).

Harms, V. et al. (1991). Properties of ^{22}Ne(α,n)^{25}Mg resonances. *Physical Review C*, 43(6):2849.

Healy, M.J.F. (1997). Minimising carbon contamination during ion beam analysis. *Nuclear Instruments and Methods in Physics Research B*, 129:130–136.

Heine, M. et al. (2018). The STELLA apparatus for particle-gamma coincidence fusion measurements with nanosecond timing. *Nuclear Instruments and Methods in Physics Research A*, 903(1).

Heine, M. et al. (2022). Direct measurement of carbon fusion at astrophysical energies with gamma-particle coincidences. *EPJ Web Conf*, 260:01004.

Iliadis, C. et al. (2010). Charged-particle thermonuclear reaction rates: Ii. tables and graphs of reaction rates and probability density functions. *Nuclear Physics A*, 841:31–250.

Jaeger, M. et al. (2001). ^{22}Ne(α,n)^{25}Mg: The key neutron source in massive stars. *Physics Review Letters*, 87:202501.

Jayatissa, H. et al. (2020). Constraining the ^{22}Ne(α,γ)^{26}Mg and ^{22}Ne(α,n)^{25}Mg reaction rates using sub-coulomb α-transfer reactions. *Phys. Lett. B*, 802(135267).

Jiang, C. et al. (2008). Fusion hindrance for a positive Q-value system. *Physical Review C*, 78(017601).

Jiang, C. L. et al. (2018). Reaction rate for carbon burning in massive stars. *Physical Review C*, 97(1):012801.

Krasznahorkay, A. J. et al. (2016). Observation of anomalous internal pair creation in ^{8}Be: A possible indication of a light, neutral boson. *Physics Review Letters*, 116:042501.

La Cognata, M. et al. (2013). On the measurement of the ^{13}C(α,n)^{16}O s-factor at negative energies and its influence on the s-process. *The Astrophysical Journal*, 777(2):143.

Longland, R. et al. (2012). Reaction rates for the s-process neutron source ^{22}Ne+α. *Physical Review C*, 85:065809.

Martínez-Rodríguez, H. et al. (2017). Observational Evidence for High Neutronization in Supernova Remnants: Implications for Type Ia Supernova Progenitors. *The Astrophysical Journal*, 843(1):35.

Mayer, M. (1999). Simnra, a simulation program for the analysis of NRA, RBS and ERDA. *AIP Conference Proceedings*, 475(1):541–544.

Mercogliano, D. et al. (2024). The new deep-underground direct measurement of ^{22}Ne(α,γ)^{26}Mg with easγ: A feasibility study. *Galaxies*, 12(6):79.

Monpribat, E. et al. (2022). A new ^{12}C+^{12}C nuclear reaction rate: Impact on stellar evolution. *Astronomy & Astrophysics*, 660:A47.

Montagnoli, G. et al. (2020). Study of fusion hindrance in the system ^{12}C+^{24}Mg. *Journal of Physics: Conference Series*, 1643(012098).

Morales-Gallegos, L. et al. (2018). Reduction of deuterium content in carbon targets for ^{12}C+^{12}C reaction studies of astrophysical interest. *European Physical Journal A*, 54(8):132.

Nippert, J. et al. (2024). Recent results on direct measurement of the ^{12}C+^{12}C fusion cross section at deep sub-barrier energies with STELLA. *Acta Phys Pol B Proc Suppl*, 17:3–A33.

Notani, M. et al. (2012). Correlation between the ^{12}C+^{12}C, ^{12}C+^{13}C, and ^{13}C+^{13}C fusion cross sections. *Physical Review C*, 85(014607).

Oliva, A. et al. (2023). Study of the ^{12}C+^{16}O fusion reaction in carbon burning via the Trojan Horse Method. In *Nuclear Physics in Astrophysics - X (NPA-X 2022)*, volume 279 of *European Physical Journal Web of Conferences*, page 11015.

Patterson, J. et al. (1971). Experimental investigation of ^{16}O + ^{12}C nuclear burning at stellar energies. *Nuclear Physics A*, 165(3):545–559.

Piatti, D. (2024). Laboratory for underground nuclear astrophysics. In *European Physical Journal Web of Conferences*, volume 297 of *European Physical Journal Web of Conferences*, page 01009.

Picollo, F. et al. (2021). Creation of pure non-crystalline diamond nanostructures via room-temperature ion irradiation and subsequent thermal annealing. *Nanoscale Advances*, 3(14):4156–4165.

Sargsyan, V. et al. (2022). Constraints on the appearance of a maximum in astrophysical S-factor. *Physics Letters B*, 824(136792).

Schatz, H. et al. (2014). Strong neutrino cooling by cycles of electron capture and β-decay in neutron star crust. *Nature*, 505:62–65.

Sen, A. et al. (2019). A high intensity, high stability 3.5 MV singletron accelerator. *Nuclear Instruments and Methods in Physics Research B*, 450:390–395.

Spartà, R. et al. (2022). Neutron-driven nucleosynthesis in stellar plasma. *Frontiers in Physics*, 10(896011).

Spillane, T. et al. (2007). ^{12}C+^{12}C fusion reactions near the gamow energy. *Physics Review Letters*, 98(12):122501.

Spitaleri, C. et al. (2019). Astrophysics studies with the Trojan Horse method. *The European Physical Journal A*, 55:1–29.

STAR (2021). Solid Targets for Astrophysics Research. `https://www.chetec-infra.eu/jra/star/`.

Tan, W. et al. (2024). Coincident measurement of the ^{12}C+^{12}C fusion cross section via the differential thick-target technique. *Physical Review C*, 110:035808.

Tan, W. P. et al. (2020). New measurement of ^{12}C+^{12}C fusion reaction at astrophysical energies. *Physics Review Letters*, 124(19):192702.

Tudor, D. et al. (2020). A facility for direct measurements for nuclear astrophysics at ifin-hh - a 3 MV tandem accelerator and an ultra-low background laboratory. *Nuclear Instruments and Methods in Physics Research A*, 953(163178).

Tumino, A. et al. (2018). An increase in the ^{12}C+^{12}C fusion rate from resonances at astrophysical energies. *Nature*, 557(7707):687–690.

Tumino, A. et al. (2021). The Trojan Horse method: a nuclear physics tool for astrophysics. *Annual Review of Nuclear and Particle Science*, 71(1):345–376.

Tumino, A. et al. (2025). Indirect methods with transfer reactions: The Trojan Horse method and the asymptotic normalization coefficient. *Progress in Particle and Nuclear Physics*, 143:104164.

Weaver, T. A. and Woosley, S. (1993). Nucleosynthesis in massive stars and the ^{12}C(α, γ)^{16}O reaction rate. *Physics Reports*, 227(1-5):65–96.

Wiescher, M. et al. (2012). Critical Reactions in Contemporary Nuclear Astrophysics. *Annual Review of Astronomy and Astrophysics*, 50:165–210.

Wiescher, M. et al. (2023). The resonances in the ^{22}Ne+α fusion reactions. *European Physical Journal A*, 59(1):11.

Woosley, S. et al. (1971). Astrophysical Importance of the Reaction ^{12}C+^{16}O. *Physical Review Letters*, 27(4):213–216.

Zhang, N. et al. (2020). Constraining the ^{12}C+^{12}C astrophysical s-factors with the ^{12}C+^{13}C measurements at very low energies. *Physics Letters B*, 801(135170).

Zickefoose, J. et al. (2018). Measurement of the ^{12}C(^{12}C,p)^{23}Na cross section near the gamow energy. *Physical Review C*, 97(6):065806.